ADVANCED FUNCTIONAL MATERIALS
www.afm-journal.de

Engineered 3D Silk-Based Metastasis Models: Interactions Between Human Breast Adenocarcinoma, Mesenchymal Stem Cells and Osteoblast-Like Cells

*Sarmistha Talukdar and Subhas C. Kundu**

Bone metastasis occurs in 70% of breast cancer patients and is a frequent cause of morbidity in cancer patients. A delicate balance exists in the bone microenvironment, but the functional dynamics underlying the tumor cell-microenvironment interactions remain poorly understood. 3D in vitro model systems of metastasis can throw new light on this phenomenon. Silk protein fibroin scaffolds, are cytocompatible for 3D cancer cell culture. They are structurally more resistant to protease degradation than other native biomaterials making these matrices suitable for cancer modeling. In this report, human breast adenocarcinoma cells, human osteoblast like cells and mesenchymal stem cells are co-cultered. Cancer cells and osteoblast-like cells are found to interact through secreted products. Decreased population of osteoblast-like cells and mineralization of extracellular matrix are observed as a result of co-culture. Significantly increased migration of breast cancer cells is observed in the bone-like constructs than in non-seeded scaffolds. The co-culture constructs show significant increase in drug resistance, invasiveness and angiogenicity. Co-culture of breast cancer cells with osteoblast like cells and mesenchymal stem cells also indicate that the interaction of cancer cells with bone microenvironment varies with spatial organization, presence of osteogenic factors as well as stromal cell type. Here, results show that 3D in vitro co-culture models is possibly a better system to study and target cancer progression.

1. Introduction

Cancer is a complex disease where tumor cells are the leading cause of pathogenesis, supported by diverse normal cells that can be recruited to aid their malignant progression. Normal cells can have both positive and negative influence on the tumor. The fate of cancer prevention or promotion is dependent to a large extent on the homeostatic or aberrant cell-microenvironment interactions respectively.[1] Cancer cells can co-opt or modify these normal cells surrounding them to produce a variety of growth factors, chemokines and matrix degrading enzymes that enhance the tumor proliferation and invasion.[2] Approaches in which tumor and stromal cells are considered may prove a more effective way of cancer chemotherapy. Tumor cells are susceptible to mutations and thus have the ability to become drug resistant. However, a delicate balance exists in the tumor microenvironment, between its tumor–inhibitory and tumor promoting functions.[2] Increasing evidence supports the role of the tumor microenvironment in conferring drug resistance as a major cause of relapse and incurability of cancer. Tumor-tumor cell interaction, tumor-stromal cell interaction, as well as tumor-extracellular matrix (ECM) interaction, chemical and mechanical cues play important roles in each step of cancer pathogenesis, as well as direct contact mediated drug resistance.[1–4] Environment mediated-drug resistance (EM-DR) is the sum of cell adhesion mediated drug resistance (CAM-DR) and soluble factor mediated drug resistance (SM-DR) produced by tumor host interaction.[5] However, the functional dynamics underlying the cell-microenvironment interactions remain poorly understood.[1]

Bone metastasis occurs in 70% of breast cancer patients and is a common cause of morbidity in cancer patients.[6,7] Tumor cells arrive at secondary sites at high rates, but metastatic cells need a suitable, usually stereotypical environment to survive and proliferate;[2,8–10] the pattern of metastasis formation is not random. This underlines the emphasis of tumor microenvironment in cancer cell survival and metastasis. Cancer cells, though adept at exploiting their primary origin, need to survive in the new microenvironment during secondary tumor formation. This ability to metastasize is the most fearsome aspect of cancer as it is responsible for most of the cancer deaths. To form a full-fledged metastases, a cancer cell must complete the metastatic cascade, a series of well-defined steps including local invasiveness, cell detachment, vascular invasion, circulation or transport, cell arrest, extravasation, survival, proliferation and angiogenesis.[11]

Cancer cells may orientate along soluble chemo-attracting factors or insoluble ECM components, at the site of cell attachment, a process referred to as haptotaxis.[11] The local expression of the chemoattractants might guide the chemokine receptor expressing tumor cells to specific destinations, resulting

S. Talukdar, Prof. S. C. Kundu
Department of Biotechnology
Indian Institute of Technology
Kharagpur 7213 02, India
E-mail: kundu@hijli.iitkgp.ernet.in

DOI: 10.1002/adfm.201300312

in chemotaxis and invasion of cancer cells.[10,12,13] Growth factor signaling can promote adhesion formation at the leading front of the cell. Bone is a rich source of diverse group of growth factors such as insulin-like growth factor 1 (IGF-I). In metastatic breast carcinoma cells, the metastatic potential has been related to IGF-I induced chemotaxis. In contrast non-metastatic cells tumor cells do not show chemotactic potential.[11,14] Cell motility along with tightly regulated matrix proteolysis by the matrix metalloproteinases (MMPs) secreted by the cancer cells are required for effective invasive growth.[11,15] In addition, MMPs also help cancer cell chemotaxis by co-operating with integrins to promote cell migration.[11,16,17]

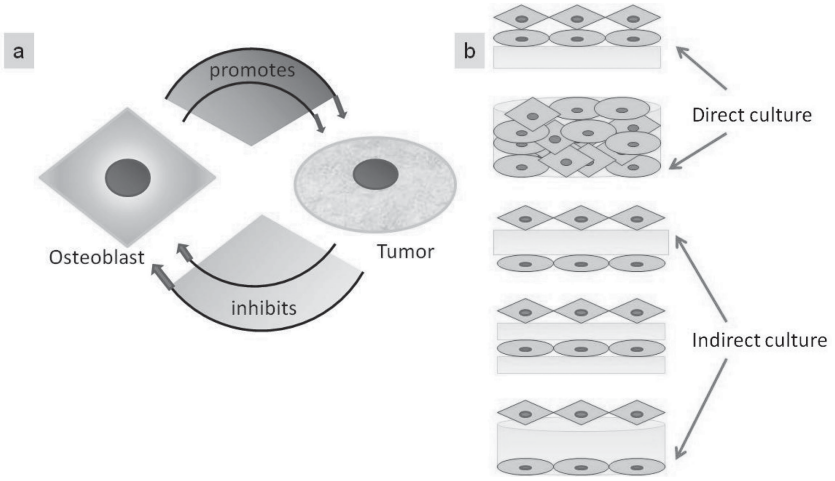

Scheme 1. Diagrammatic representation of a) influence of osteoblasts and cancer cells on each other and b) possible co-culture methods to study their interactions.

Normal bone density is dynamically regulated by the homeostasis between osteoblasts that lay down bone, and osteoclasts that degrade bone.[2] Breast cancer metastases form secondary tumors, interfere with bone remodeling and cause osteolytic lesions by stimulating the formation and activity of osteoclasts.[7,18] These lesions cause severe pain, pathological fracture, hypercalcemia, nerve compression, and an overall poor clinical prognosis.[7,19] A variety of growth factors and cytokines drive the vicious cycle of bone metastasis, such as vascular endothelial growth factor (VEGF), IL-8, IL-11, parathyroid hormone-related protein (PTHrP), have pro-migratory and osteoclastogenic activities that decouple the homeostatic balance between bone formation and bone resorption.[7,19] The osteoclastic lineage is regulated by colony stimulating factor-I (CSF-I) which under the influence of receptor activator of NF-kB ligand (receptor activator of nuclear factor kappa-B ligand, RANKL), causes differentiation of progenitor cells in the bone marrow into osteoclasts.[10,20–22] The breast cancer cells produce CSF-I along with PTHrP and tumoor necrosis factor-alpha (TNF-α), which activate RANKL and inhibit osteoprogerin (a soluble RANKL receptor) synthesis, resulting in elevated count and activity of osteoclasts.[10,23,24] Resorption of bone elevates PTHrP secretion by the cancer cells, intensifying osteolysis. Calcium sensing receptor (CaR) regulates calcium homeostasis and PTHrP secretion.[25] PTHrP activity also increases the level of Ca^{2+} and tumor growth factor (TGF) β within the bone microenvironment evoking further worsening osteolysis.[26] Mesenchymal stem cells (MSC) form a key component of the bone microenvironment as the precursor cells of the bone marrow stromal cells, and their presence also influences cancer development. There are evidences which show that MSC inhibit tumor cells.[23,27] Other studies indicate that mesenchymal stem cells facilitate cancer cell entry into the bone marrow[28] and may accelerate tumor growth by generating cytokine networks that regulate the breast cancer stem cell population.[23] Some groups are of the opinion that there is stark difference in influence of MSC on cancer in vitro and in vivo, and that the clinical use of MSC for treatment of malignant diseases should be handled with extreme caution.[29] Studying such a myriad of influences of bone microenvironment on metastasis may shed light on mechanisms that lead to cancer progression and suggest better modes of treatment.

Tissue engineering has the potential to revolutionize basic and applied cancer research by further advancing our understanding of tumorigenesis.[30–33] To study the response of metastasizing cancer cells to external stimuli, co-culture is an absolute necessity. Co-culture of the involved cells can be either direct or indirect. Such co-culture models can help in understanding co-evolution of both the cancer cells and the surrounding cells (**Scheme 1**). These tissue engineered tumor modeling systems offer a more convenient, mechanically stable system to study, analyze, prevent and even implant tumors. *Antheraea mylitta (A. mylitta)* silk fibroin protein scaffolds offer a platform that is cytocompatible, whose mechanical strength, porosity and degradability may be tailored[34–36] for the study of tumor microenvironments.[37] The *A. mylitta* silk protein fibroin scaffolds (2%) are highly porous with pore sizes of 150–200 μm. Scaffolds (2%) measuring 10 mm in diameter and 10 mm in height posess a compressive strength of 84 kPa,[38] which is higher than other reported naturally derived materials used for 3D scaffold fabrication (e.g., collagen scaffolds: 15 kPa and chitosan scaffolds: 45 kPa, respectively).[39] Scaffolds of 6.4 mm in diameter and 2 mm thickness showed compressive modulus of 5.2 kPa at frequency of 0.005 Hz, and dynamic stiffness of 8 kPa at frequency of 1.5 Hz and the cell-seeded construct can reach a dynamic stiffness of 42.5 kPa.[36] This non-mulberry silk protein fibroin also naturally possesses Arg-Gly-Asp (RGD) sequences (GenBank: AY136274.1),[40] which contributes to its excellent cytocompatibility. Its non-cytotoxic property and low level of inflammatory response[41,42] make it an excellent material for tissue engineering. These silk protein fibroin scaffolds (2%) are very stable, they do not degrade in phosphate buffered saline (PBS) and the matrices were completely degraded by proteases only after 28 days of incubation.[34] These biophysical properties can play a very important role in long term cancer culture. Cancer cells produce matrix degrading enzymes such as collagenases, which can easily degrade matrices made of collagen or other native matrix material, making it difficult for long term cell culture. Moreover, this degradation can cause loss of biophysical properties, like scaffold architecture and stiffness of the 3D culture system. For this reason, it may be

difficult to study aggressive, metastatic cell lines within a 3D domain which is susceptible to degradation. *A. mylitta* silk fibroin properties suggest it may be a good candidate for cancer engineering. Its high compressive strength can contribute to the matrix stiffness, an important regulator of malignant transformation, growth, motility and invasion, cancer cell survival, and metastatic dissemination.[43,44] Matrix rigidity can modulate tissue fibrosis and stiffness to force focal adhesions, growth factor signaling and breast malignancy.[45] The measured shear stiffness of the tumors ranged from 18 to 94 kPa (mean, 33 kPa). The shear stiffness measurements of adipose breast tissue in the breast cancer patients ranged from 4 to 16 kPa, with a mean of 8 kPa[46] which is close to the stiffness observed for *A. mylitta* (2%) scaffolds. We have observed earlier,[37,47] that silk fibroin scaffolds provide an amenable environment for longterm cancer culture, and the cancer cells cultured on these scaffolds show more aggressiveness than those cultured on some of the other 3D culture systems. The constructs also show avascular tumor like morphology, which also contributes to their aggressiveness and drug resistance.[47] Human stem cells are also reported to successfully differentiate by osteogenesis on *A. mylitta* silk scaffolds,[48] making them a good candidate to study bone metastasis. Based on these findings, in this study, we develop a co-culture based metastasis model to study interactions between human breast cancer cell line (HBCC, breast adenocarcinoma MDA-MB-231), human osteoblast-like cell line (HOLC, MG-63) and mesenchymal stem cells, using non-mulberry *A. mylitta* fibroin scaffolds.

2. Results and Discussion

2.1. Morphology of Non Co-Cultured and Co-Cultured Cells

Rhodamine-phalloidin, fluoresein isothiocyate conjugated with phalloidin (FITC-phalloidin) and Hoechst 33342 staining was performed to observe the cell attachment, spreading, morphology, proliferation and distribution cells. Both non co-cultured and directly co-cultured 3D constructs showed the presence of well defined cytoskeleton and nucleus in all the cells (**Figure 1**a–c). The scaffold stained with Hoechst 33342 showed well defined pores (Figure 1d). Z-sections of the seeded scaffolds were stacked to obtain the complete distribution of cells at a particular microscopic field. Stacked Z-sections allowed observation of the cells growing inside the 3D scaffolds. Cell morphology on 2D tissue culture plates show the healthy morphology of cells prior to seeding (Figure 1d,e). HBCC cells did not show any aberrant morphology when cultures in StemPro media (Figure 1f).

Human mesenchymal stem cells (HMSCs) show healthy morphology on 3D scaffolds after 7 days of culture, with well attached cells as shown by the intense development of actin microfilaments. The cells are evenly distributed and completely filled up all the pores of the scaffold (Figure 1g). HMSCs under osteogenic differentiation media also show well developed tissue formation (Figure 1h).

2.2. Cell Response to Conditioned Media

To study whether extracellular factors secreted by the human breast cancer cells (HBCCs) and human osteoblast-like cells (HOLCs) affect the cell morphology, attachment, spreading and metabolic activity, the two cell lines were seeded separately in 6 well tissue culture plates. Cell attachment studies were carried out on 2D instead of 3D. The main reason for conducting the experiment in 2D is that it is very difficult to obtain all the cells from the 3D mesh-like matrix. HBCCs cultured in : Dulbecco's modified eagle medium (DMEM)/F-12 and HOLCs cultured in minimum essential media (MEM), untreated with any conditioned media were considered as controls for HBCC and HOLC cultures respectively (**Figure 2**). Conditioned media (CM) of HBCCs was used to treat HOLCs

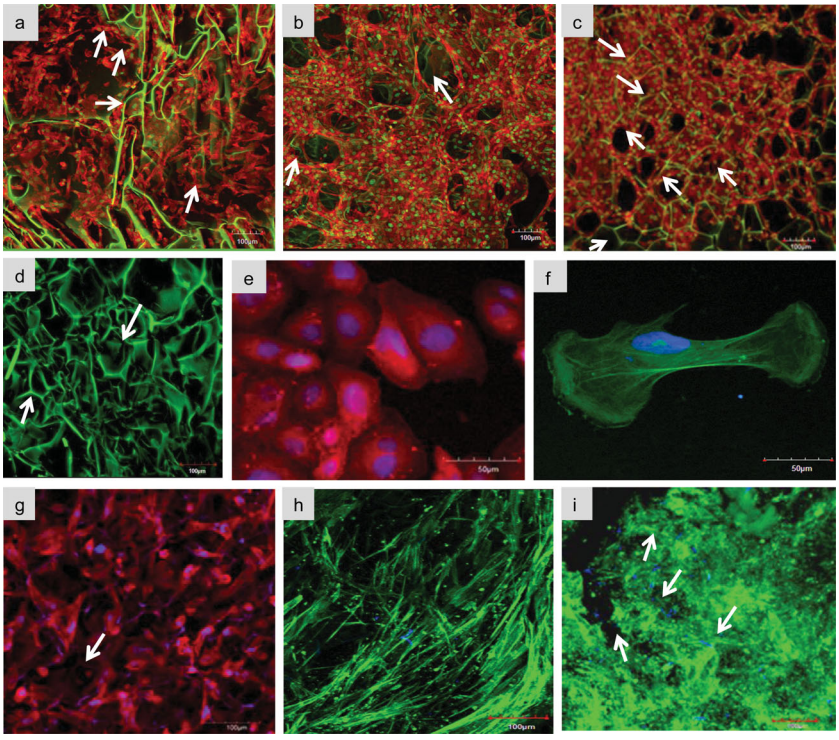

Figure 1. Confocal laser scanning fluorescence microscopy images showing cell attachment, spreading, morphology, proliferation and distribution in 2D and 3D cultures. a) HBCC b) HOLC c) direct co-culture of HBCC and HOLC (1:1) on *A. mylitta* fibroin 3D scaffolds and d) non-seeded porous *A. mylitta* silk fibroin scaffold; e) HBCC f) HMSC on 2D tissue culture plates; g) HBCC cultured in StemPro media, h) HMSC cultured in StemPro media i) HMSC cultured in osteogenic differentiation media on 3D fibroin scaffolds. The HBCC and HOLC are stained with Rhodamine-phalloidin (red) and Hoechst 33342 (green and blue) for the nuclei. HMSC are stained with FITC phalloidin (green) and Hoechst 33342. The pores where visible are indicated by white arrows. Scale represents 100 µm in (a–c) and (f–h), and 50 µm in (d–e).

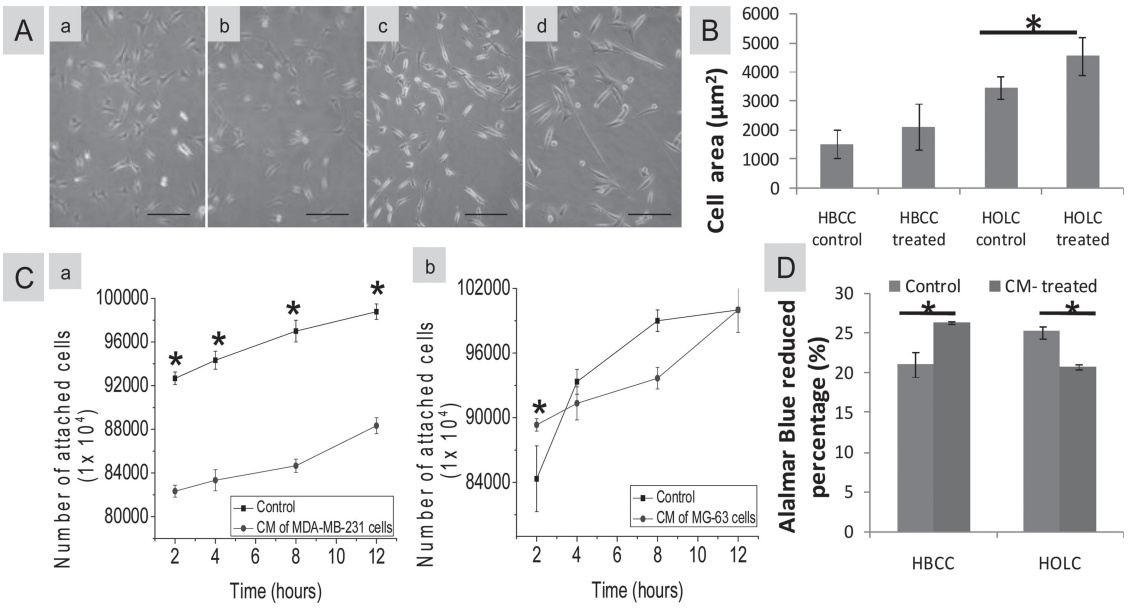

Figure 2. Response of cells to conditioned media (CM). A). Effect of CM on 2D cell morphology of a) HBCCs without CM treatment, b) HBCCs treated with CM of HOLC, c) HOLC without CM treatment, d) HOLC treated with CM of HBCC. Scale bar represents 250 μm. B). Effect of CM on cell spreading. C). Effect of CM on attachment of cells on 2D tissue culture plates a) HOLC treated with CM of HBCC; controls are untreated b) HBCCs treated with CM of HOLC; controls are untreated. D). Effect of CM on HBCC and HOLC viability in 3D scaffolds.

cells for 24 h and vice versa. Observable differences were noted in the CM-treated samples in comparison with controls. The morphology of the HOLC became elongated to 2–3 times of their original length, cell spreading of HOLCs treated with HBCC-CM, was significantly more than that of the control (Figure 2Ac,d,B). After 12 h of culture, significantly less number of HOLCs had attached in presence of HBCC-CM than the HOLC control (Figure 2Ca), and the number HBCCs attached initially in HOLC-CM was more than the untreated HBCC control (Figure 2Cb). To study the effect of CM on metabolic activity, the two cell lines were seeded separately on scaffolds. Metabolic activity of HBCCs was also observed to be more in presence HOLC-CM, whereas the opposite was observed in case of HOLC cells treated with HBCC-CM. Osteolytic, metastatic breast cancer cells decreased the viability of HOLCs (Figure 2D). The results show that HBCCs and HOLCs indirectly modulated each others' activity. The CM of HOLC had a stimulatory effect on HBBC viability and initial attachment, whereas the CM of HBCC had an inhibitory effect HOLC attachment and viability. Breast cancers express cytokines (such as IL-1, IL-6, leukemia inhibitory factor (LIF), prostaglandin E2 (PGE2), tumor necrosis factor-α (TNFα), TGF-β, PTHrP, and osteobtasts are known to respond these osteolytic agents through an alteration in growth rate and/or by secreting osteoclast-modulating factor(s).[51,52] These factors play an important role in the formation of the vicious self-feeding cycle of tumor mediated osteolysis,[53] the details of which are not clearly known.[54] TGF-β is reported to cause cell elongation in osteoblasts,[55] which may be responsible for the abnormal morphology observed in HOLCs treated with the conditioned media of HBCCs. Since regulation of cell shape is a central route that controls tissue morphogenesis, cell migration, differentiation, proliferation, and survival by influencing the expression of genes central to these processes,[55] it could be possible that TGF-β-induced osteoblast elongation contributes to several aspects of TGF-β function in various events of breast cancer mediated osteolysis. There could be many possible mechanisms for inhibition of osteoblasts by cancer cells, and stimulation of cancer cells by osteoblasts, emphasizing the need of a model system to investigate their interactions.

2.3. Growth of Cancer Cells, Osteoblast-Like Cells, and Co-Culture

HBCCs and HOLCs were trypsinized, and stained red and green respectively. These cells were then mixed in the ratio of 1:1 and seeded on *A. mylitta* fibroin 3D scaffolds keeping the total population as 2×10^6 cells. Both the cell lines were able to attach (**Figure 3**a), spread and grow throughout the period of co-culture, filling the pores of the scaffold (Figure 3b–f). However, gradual increase in the population of HBCCs and decrease in HOLCs were observed, even though the doubling time of both the cell lines was same. The HOLCs formed small clusters surrounded by the smaller HBCCs (Figure 3b,c,e,f). The results probably indicate another feature of tumor mediated osteolysis, where aggressive breast cancer cells spread in the bone microenvironment and inhibit the growth of osteoblasts. The colonization and growth of cancer metastases in the bone depends on a cooperative interaction of the cancer cells with the host cells in the bone microenvironment.[53] The complex bone microenvironment produces an array of cytokines and growth factors favorable for cancer cells.[56] Their interaction with osteoblasts further induces the release of cytokines that promote cancer growth[53,56] Moreover breast cancer cells are also known to cause apoptosis[53] and

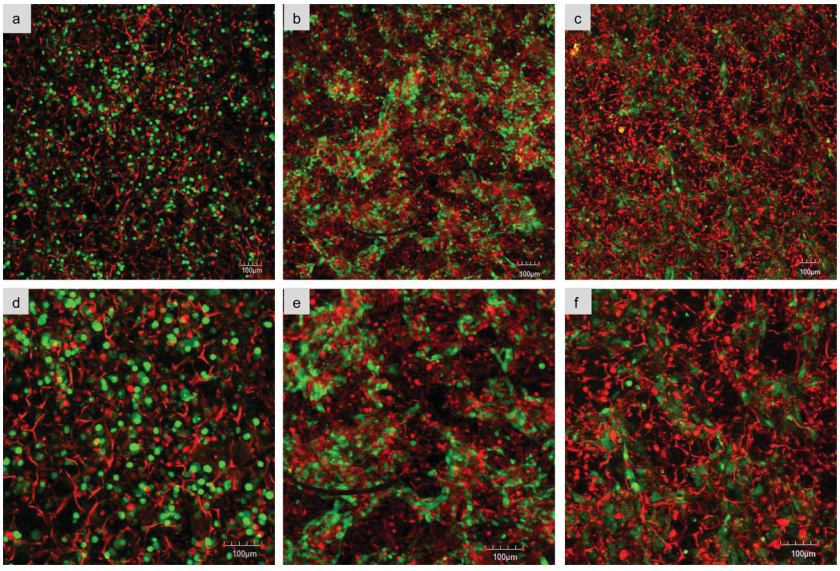

Figure 3. Confocal laser scanning fluorescence microscopy images representing live stained direct co-culture of HBCCs (red) and HOLC (green) growing inside the 3D scaffolds, initially seeded in the ratio of 1:1 on a,d) day 1, b,e) day 3, c,f) day 5. Scale bar = 100 μm.

inhibition of differentiation in osteoblasts.[57] In this 3D co-culture model of HBCC and HOLC, the cells probably interact in a similar fashion leading to gradual proliferation of HBCCs and decrease in HOLC population.

Metabolic activity of 3D co-cultures and mono-cultures was studied by Alamar Blue assay as a function of time. Gradual proliferation was observed in all the cultures (**Figure 4**a). HBCCs and co-cultured cells proliferated 4 folds, and HOLCs proliferated 3 folds to the data observed on day 1 (**Figure 5**c). 3D HBCC and co-culture showed similar growth kinetics, whereas 3D HOLC culture showed lesser growth and proliferation than the other two cultures (Figure 4b,c). The similarity in the growth profiles of HBCC and co-culture may be due to increase in the number of HBCCs and simultaneous decrease of HOLCs in the co-culture (Figure 3).

2.4. Osteolytic Effect of Cancer Cells on the Mineralization of Co-Culture Constructs

The bone ECM is a composite material that comprises of an inorganic mineral phase dispersed throughout an organic matrix of collagen. The inorganic component of bone is primarily composed of crystalline calcium phosphate.[58] Alkaline phosphatase is another biochemical indicator of mineralized ECM.[59] Mineralization of bone is essential for its hardness and strength and the process involves production of calcium phosphate crystals by osteoblasts in precise amounts within the bone's ECM. Improper regulation of this process can compromise bone health. We studied the effect of coculturing HBCCs with HOLCs on the ECM mineralization. The cultures were grown for a period of 21 days and sections were cut. Haematoxylin and eosin staining of sections showed well developed tissue formation (Figure 5A). Alizarin red staining of the sections showed mineralization and calcium nodule formation in osteoblast-like constructs (Figure 5Bb). Calcium deposition in the osteoblast-like constructs was much more intense and consistently distributed than that of the tumor constructs (Figure 5Ba,b). The calcium staining in the co-cultures was not evenly distributed, with patches of heavy deposition and large un-stained regions (Figure 5Bc). Differences were also observed in the alkaline phosphatase activity in the supernatant media of the cultures. There was a slight decrease between osteoblast-like and co-culture constructs (Figure 5C). The changes of the physical properties of the constructs were marked. The thickness of osteoblast-like constructs was significantly more than that of tumor and co-culture constructs (Figure 5D). This is probably due to the presence of large amount of mineralized ECM in the osteoblast-like tissue constructs.

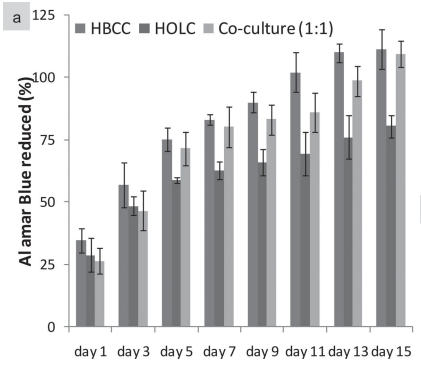

b

Normalized to co-culture day 1 data	day 1	day 15
MDA-MB-231	1.31 ± 0.14	4.21 ±0.16
MG-63	1.09 ± 0.24	3.04 ±0.06
Co-culture (1:1)	1.00 ± 0.35	4.13 ±0.14

c

Normalized to co-culture day wise data	day 15
MDA-MB-231	1.02 ± 0.08
MG-63	0.74 ±0.11
Co-culture (1:1)	1.00 ±0.18

Figure 4. Cell viability, growth and proliferation of co-cultures and mono-cultures of HBCCs and HOLCs by a) Alamar blue assay, b) data obtained on day 15 normalized to the co-culture data obtained on day 1 by Alamar Blue assay, c) data obtained on day 15 normalized to the co-culture data obtained on day 15 by Alamar Blue assay.

2.5. In Vitro Migration of Breast Cancer Cells Towards Engineered Bone Tissue Constructs

To study migration of cells into osteoblast-like constructs, pre-labeled HBCCs (red) and HOLCs (green) were cultured separately for 7 days and then co-cultured indirectly. A non-seeded fibroin scaffold was used as control. Migration of HBCCs through the culture media against the gravity and into the osteoblast-like constructs was observed from day 1 (4.6%; **Figure 6**a), which gradually increased upon increasing the duration of co-culture (23%, 39% on day 3 and day 5 respectively; Figure 6b,c). On day 7, a large number of cancer cells were observed surrounding the HOLCs, and a few moving inwards of the HOLC clusters (44.3%; Figure 6d). No

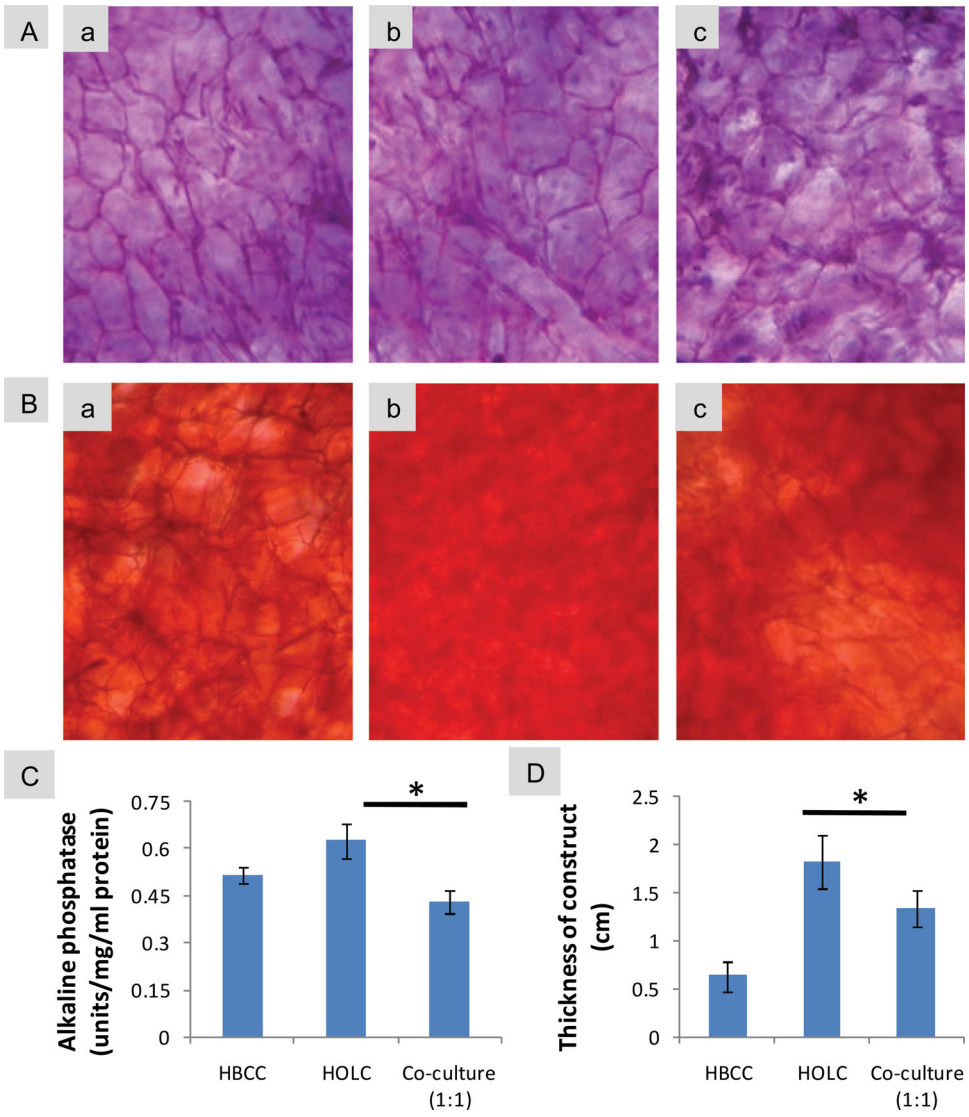

Figure 5. Analysis of histological, biochemical and biophysical aspects of HBCC, HOLC mono-cultures and co-cultures. A). Haemotoxylin and eosin staining of a) 3D HBCC culture b) 3D HOLC culture, and c) HBCC: HOLC co-culture. B). Saffranin-O staining of a) 3D HBCC culture b) 3D HOLC culture, and c) HBCC: HOLC co-culture. C) Alkaline phosphatase of 3D HBCC culture, 3D HOLC culture, and HBCC: HOLC co-culture. D) Thickness of 3D HBCC culture, 3D HOLC culture, and HBCC: HOLC co-culture constructs.

HBCCs were observed in the control on day 1, and on day 7 a few small clusters were seen (Figure 6e–g). The migration of HBCCs is probably chemotactic.

It has long been unclear as to why particular cancers preferentially metastasize to certain sites, though several theories are postulated by several groups of researchers. Chemokine receptors such as CXCR4, CCR, and calcium sensing receptors (CASR) are expressed on the surface of breast cancer cells and their ligands are highly expressed at sites associated with breast cancer metastases.[60,61] Some are of the opinion that stromal cell-derived factor-1[62] and osteonectin[63] may be involved in chemotactic, directed migration of tumor cells from their primary site via the circulation to the preferential sites of metastases. Development of clinically appropriate models of cancer invasion and metastasis can not only throw new light on this complex process but also help in defining new targets of cancer therapy.

2.6. Metabolic Activity of Co-Cultures with and Without the Presence of Osteogenic Differentiation Media

Metabolic activity of 3D co-cultures and monocultures with and without osteogenic differentiating media was studied by Alamar Blue assay as a function of time. Co-cultures were cultured in media composition of DMEM/F12: StemPro in the ratio of 1:1 respectively, and the initial cell seeding ratio of HBCC: HMSC was also 1:1. Gradual proliferation was observed in all the cultures. There was no significant difference in the proliferation of 3D HMSC, HBCC and co-cultured constructs cultured

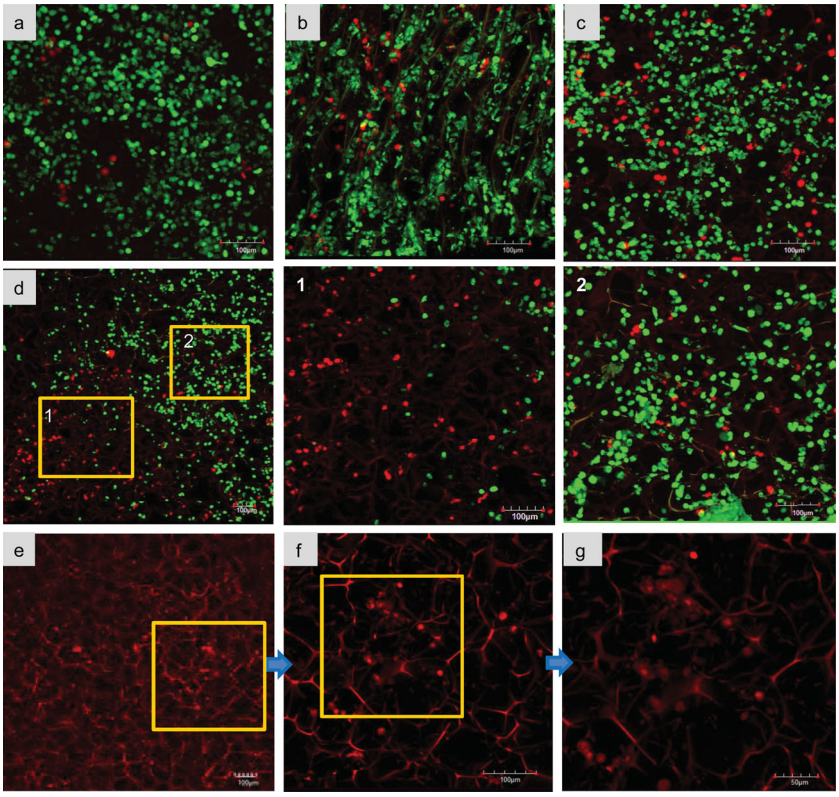

Figure 6. Confocal laser scanning fluorescence microscopy images representing live stained indirect co-culture of HBCCs (red) and HOLC (green) on a) day 1, b) day 3, c) day 5, d) day 7. Inset 1 and 2 are magnified to show different regions of the osteoblast-like construct with varying number of HBCCs. e–g) HBCCs on non-seeded scaffolds on day 7. Scale bar represents 100 µm.

without osteogenic media, even after 21 days of growth. There was also no significant difference in the proliferation of 3D HMSC, HBCC constructs cultured with osteogenic media (**Figure 7**a), with very slight increase in comparison with day 1 data (Figure 7c). The proliferation of HMSCs and HBCCs was slightly more than that of the co-cultures (Figure 7d). However, significant increase in proliferation was observed in the co-cultures of HMSC and HBCC in comparison with mono-cultures, in presence of osteogenic media (Figure 7b,d).

2.7. Invasiveness, Angiogenicity and Bone Homeostasis in Co-Cultures

To study the effect of 3D co-culture on production of invasive and angiogenic factors, HBCCs were co-cultured with HOLCs, and HMSCs (with and without osteogenic media) on porous silk fibroin scafolds. The direct co-culture seeding was of two types: with HBCCs seeded on top of HMSCs and in the other, HBCCs and HMSCs/HOLCs were thoroughly mixed together and then seeded on 3D scaffolds. The seeding ratio of HBCC: HOLC/HMSC was always 1:1. 3D mono-cultures were considered as controls. HBCC:HOLC co-cultures were assayed for VEGF and IL-8, and HBCC:HMSC co-cultures were assayed for TGF-β2 and basic fibroblast growth factor (bFGF). Significant increased production of VEGF and IL-8 was observed in co-cultures of HBCCs and HOLCs (1:1) (**Figure 8**a). There was no significant difference in TGF-β2 and bFGF production among the 3D cultures of HBCCs, and HBCC on top of HMSC co-cultures. However the production of TGF-β2 and bFGF was significantly higher in case of the mixed co-cultures (Figure 8b). HMSCs produced greater amount of TGF-β2,

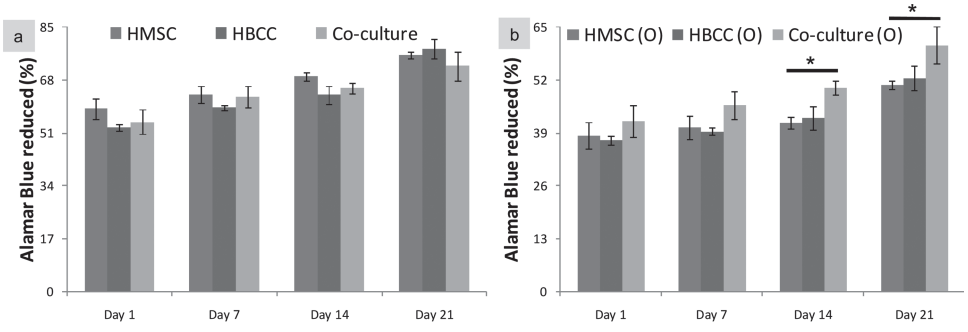

c

Normalized to co-culture day 1 data	Day 1	Day 21
HMSC	1.08 ± 0.07	1.39 ± 0.08
HBCC	0.97 ± 0.04	1.43 ± 0.06
Co-culture	1 ± 0.05	1.33 ± 0.05
HMSC (O)	0.91 ± 0.08	1.21 ± 0.02
HBCC (O)	0.89 ± 0.03	1.25 ± 0.06
Co-culture (O)	1 ± 0.09	1.47 ± 0.08

d

Normalized to co-culture day wise data	Day 21
HMSC	1.45 ± 0.16
HBCC	1.49 ± 0.18
Co-culture	1 ± 0.2
	Day 21
HMSC (O)	0.89 ± 0.02
HBCC (O)	0.91 ± 0.05
Co-culture (O)	1 ± 0.05

Figure 7. Metabolic activity of HMSC, HBCC and co-cultures a) without osteogenic media b) with osteogenic media; c) data obtained on day 21 normalized to the co-culture data obtained on day 1 by Alamar Blue assay, d) data obtained on day 21 normalized to the co-culture data obtained on day 21 by Alamar Blue assay. HMSC (O), HBCC (O) and co-culture (O) indicates their growth in presence of osteogenic media.

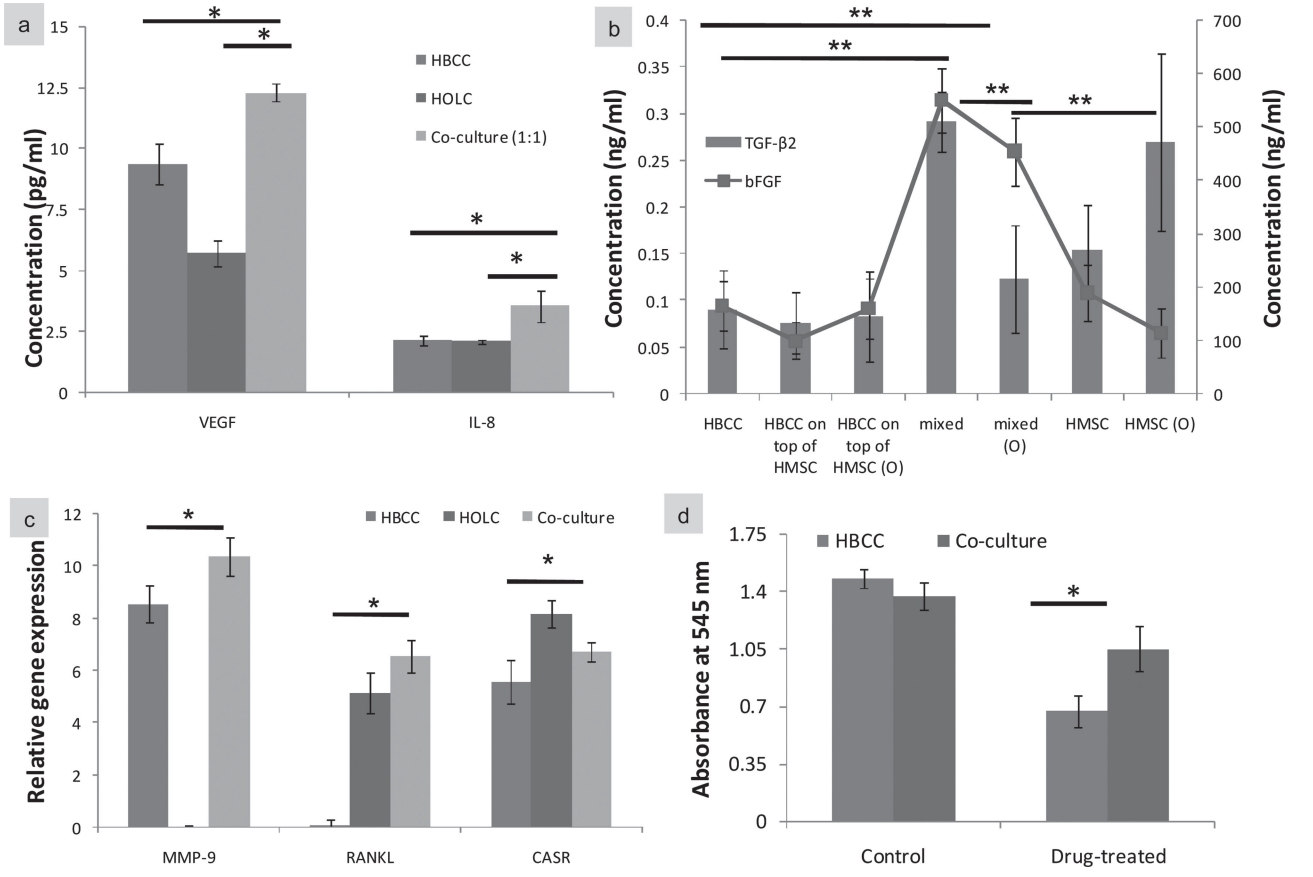

Figure 8. Expression of invasive, angiogenic and bone homeostasis factors of 3D mono-cultures and co-cultures a) VEGF and IL-8 production in HBCC, HOLC mono-cultures and co-cultures; b) TGF-β2 and bFGF production in HBCC, HMSC monocultures and co-cultures. c) RT-PCR analysis of HBCC, HOLC mono-cultures and co-cultures for the expression of MMP-9, RANKL and CASR normalized to GAPDH. d) MTT assay on drug-treated and untreated cultures. HMSC (O), HBCC (O) and co-culture (O) indicate their growth in presence of osteogenic media.

and lesser amount of bFGF than the HBCCs. The presence of osteogenic media also had significantly deceasing effect on the production of TGF-β2 and bFGF in mixed co-cultures. The production of bFGF was significantly more and production of TGF-β2 was less than that of the HMSC monocultures, in presence and absence osteogenic media.

VEGF and IL-8 regulate not only cancer initiation but also progression. TGF-β has a bimodal action on cancer, it alters the microenvironment and immune responses to provide favorable conditions for cancer maintenance; however it also acts as a tumor suppressor.[64] TGF-β2 is a potent regulator of osteoclastic bone resorption,[65] production of matrix metalloproteinase-9 and epithelial-to-mesenchymal transition.[66] bFGF protein is involved in a variety of pathological conditions including angiogenesis and solid tumour growth.[67,68] bFGF is also a stemness supporting growth factor for both embryonic and cancer stem cells.[67,69] The results indicate that interaction of HBCCs with the stromal cells of the bone microenvironment vary with spatial organization (**Scheme 2**), presence of osteogenic factors as well as stromal cell type. TGF-β2 and bFGF suppression studies indicate promising therapeutic approaches for malignant tumor therapy, but the interactions need to be deeply investigated before the design of such therapeutic strategies.

RT-PCR analysis showed that RANKL and MMP-9 (matrix metalloproteinase-9) was not produced in HBCC and HOLC cultures respectively. CASR expression was seen in all the cultures, maximum being in HOLC culture. However, the co-cultures showed an increase in the expression of both MMP-9, and RANKL (Figure 8c). Osteoclast differentiation regulated by RANKL and matrix degradation induced by matrix

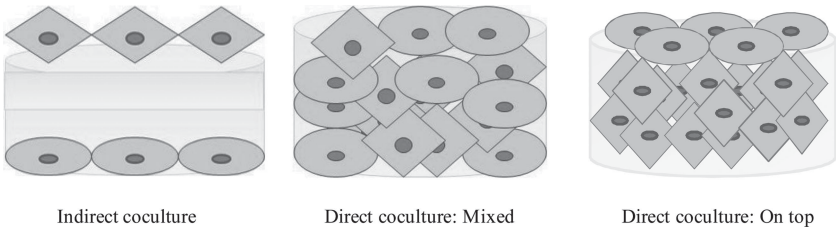

Scheme 2. Schematic representation of different spatial organizations of different cells during indirect and direct co-cultures.

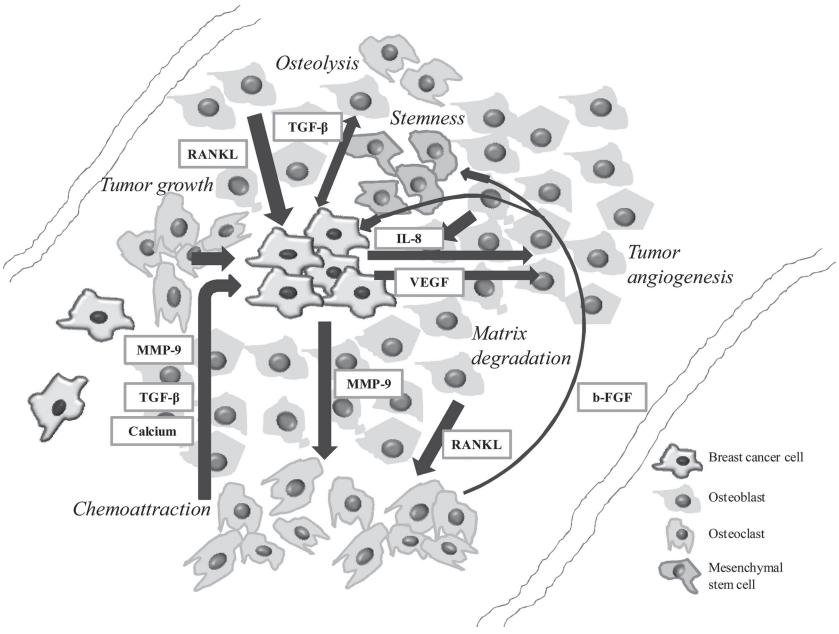

Scheme 3. Schematic representation of the probable interactions between the tumor stroma components during metastasis.

metalloproteinases are intricately involved in the process of bone resorption.[70] These results suggest that co-culture of HBCCs and HOLCs increase invasiveness and osteoclast differentiation.

Our expression study results show that complex interactions exist between the different components of the tumor stroma. **Scheme 3** shows the probable interactions between these different components as indicated by the results. The osteoclasts in the native bone microenvironment release factors like TGF-β, MMP-9, and calcium by their activity. The mesenchymal cells also release TGF-β. These chemotactically attract the metastatic cancer cells into the bone. The cancer cells secrete different osteolytic factors (MMP-9, TGF-β2, IL-8, VEGF) which degrade the bone and incite further tumor growth and progression. In response, osteoblasts release RANKL which further degrades the bone. The osteoclasts and mesenchymal stem cells secrete bFGF which maintains stemness of both cancer and mesenchymal stem cells. Apart from this, the spatial organization of these cells also regulates their interaction, tumor progression and drug resistance. These interactions between cancer cells, osteoblasts and mesenchymal stem cells are probably mimicked in our direct and indirect co-culture based metastasis model.

2.8. Acquisition of Drug Resistance by Breast Cancer Cells Upon Co-Culture with Osteoblast Like Cells

3D HBCC, and co-culture of HBCC and HOLC (1:1), were cultured for 15 days, serum starved for 24 h and then treated with Paclitaxel (25 μM). It was previously observed that 25 μM is the IC_{50} concentration of Paclitaxel for 3D HBCC cultures.[47] The drug treated cultures showed lesser viability than the untreated ones. Similar viability profile was observed in untreated HBCCs and co-cultures. However, drug-treated co-cultures showed significantly greater viability than the drug-treated HBCCs (Figure 8d). This may indicate that the microenvironment supplied by the HOLC conferred increased drug resistance to the HBCC cells in co-culture. Our earlier work on silk based tumor model (pure culture) showed significant increase in drug resistance, which was contributed mostly by the environment.[47] Environment mediated drug resistance (EMDR) is caused by signaling events commenced by factors present in the tumor microenvironment. It can be caused by ECM mediated resistance, soluble factors such as, cytokines, chemokines and growth factors secreted by tumor stroma; and by the adhesion of tumour cell integrins to stromal cells or to components of the extracellular matrix.[58] As discussed in the Section 2.7, the co-cultures are more invasive and agrressive than the pure cultures, and this may be the reason for the increased resistance to pure cultures. The results demonstrate that analyzing 3D environment mediated drug resistance could be important in the design and evaluation of new chemotherapeutic agents and prevention of acquired resistance.

3. Conclusions

3D silk scaffold based co-culture models are designed to study the interactions of human breast cancers cells with the bone microenvironment during metastasis. The media and the cell seeding ratio for direct co-culture are optimized. Extracellular secretory products of cancer cells and osteoblast-like cells are observed to affect the cell morphology, attachment, spreading and metabolic activity of each other. Breast cancer cells are found to migrate against the gravity, into engineered bone-like constructs. Significantly increased migration is observed in the bone-like constructs than in non-seeded scaffolds. Co-culture of cancer cells with osteoblast-like cells significantly increases drug resistance, invasiveness and angiogenicity, and decreases the population of osteoblast-like cells and mineralization of the constructs. Co-culture with osteoblast-like cells and mesenchymal stem cells also indicate that the interaction of cancer cells with stromal cells of the bone microenvironment vary with spatial organization, presence of osteogenic factors as well as stromal cell type. These silk based in vitro models may provide an alternative to expensive, labor-intensive animal models and may be further investigated to develop preclinical models.

4. Experimental Section

Direct and Indirect Co-Culture of Cells on 3D Silk Matrices: For direct co-culture, human breast cancer cells (HBCCs) and human osteoblast-like cells/human mesenchymal stem cells (HOLC/HMSC) were cultured at a cell ratio of 1:1 in a culture media constituted of DMEM/F-12 and MEM/StemPro (1:1); monocultures of HBCC (1:0) or HOLC, HMSC (0:1) served as controls. To study effect of HBCC on osteogenesis, HMSC

and co-cultures of HBCC: HMSC (1:1) were grown in osteogenesis differentiation media (Invitrogen, USA). Cell suspensions were prepared at appropriate ratio and cells were seeded in 24-well plates containing *A. mylitta* fibroin scaffolds at 10^6 cells/scaffold. For co-cultures, the total seeding population of all samples was kept at 2×10^6. Scaffolds were incubated at 37 °C in a humidified 95% air/5% CO_2 atmosphere. The medium was changed after every 2 days for HBCC and HOLC cultures; and after every alternate day for HMSC monocultures and HBCC-HMSC co-cultures. HBCCs were at passage 12 (P12) stage, HOLCs at P10 stage and HMSCs were at P2 stage during the study. Cell cultures were observed using an inverted light microscopy during the culture period. Measurements for all assays were performed in triplicate (n = 3).

For indirect co-culture, MDA-MB-231 cells (HBCCs) were seeded at 10^6 cells/well of a 6-well plate. MG-63 cells (HOLCs) were seeded at 2×10^6 cells on the top of each scaffold (2.5 mm thick). The cells were allowed to attach separately for 12 h. The seeded scaffolds were utilized as osteoblast-like constructs. With the help of sterile fine forceps these scaffolds were floated in wells seeded with HBCCs in a culture media of DMEM/F-12 and MEM (1:1). Mono-cultures of HBCCs or HOLCs served as controls. Scaffolds were incubated at 37 °C in a humidified 95% air/5% CO_2 atmosphere; media was changed carefully after every 2 days. Measurements for all assays were performed in triplicate (n = 3).

Cell Response to Conditioned Media: Cell attachment was calculated by counting the unattached cell population as a function of time after inoculation. Cells were trypsinized and 10^6 cells were seeded on 6-well plates (35 mm diameter well) and incubated at 37 °C in a humidified 95% air/5% CO_2 atmosphere. Seeding of the two cell lines was conducted on two separate plates. Conditioned media (CM) was prepared by centrifuging (1000 rpm for 10 min) the spent incomplete media of 75% confluent MDA-MB-231 (HBCCs) or MG-63 (HOLCs) cell cultures grown in T25-cm^2 culture flasks. All the samples were then starved by growing them in incomplete media for 24 h. The test samples of HBCCs were treated with CM of HOLCs and HOLCs cells were treated with CM of HBCCs for 48 h, whereas the controls were not treated (grown in incomplete media). Media was not changed during treatment in test samples and control. For cell attachment studies, conditioned media (CM) was prepared by centrifuging (1000 rpm for 10 min) the spent media (complete) of 75% confluent MDA-MB-231 (HBCCs) or MG-63 (HOLCs) cell cultures grown in T25-cm^2 culture flasks. Cell attachment on tisue culture plates was observed after 2, 4, 8, and 12 h of seeding. The cell culture medium was removed from the wells at mentioned intervals (2, 4, 8, and 12 h of seeding) and the unattached cells were counted with a haemocytometer. The number of cells present in the supernatant media was deducted from the initial number of cells seeded to obtain the number of attached cells.

To observe the effect of conditioned media on morphology and confluency of the two cell lines, 10^5 cells of each cell line were seeded on two separate 6-well plates. The mono-cultures were incubated at 37 °C in a humidified 95% air/5% CO_2 atmosphere for 24 h. The test samples were treated with CM whereas the controls were not treated. The mono-cultures were observed after 24 h of incubation. Ten microscopic images were randomly acquired around the central and peripheral regions. The images were analyzed with Image J (NIH) software and confluency and cell area (expressed in μm^2), were measured.

To observe the effect of CM on cell viability, scaffolds were seeded with 10^6 cells, cultured for 24 h, serum starved for the next 24 h, and then treated with CM for 24 h and assayed for viability with Alamar Blue.

Cell Viability and Proliferation of 3D Mono-Cultures and Co-Culture: Cell viability and proliferation of the 3D co-culture (1:1) and mono-cultures (1:0, 0:1) were studied using MTT and Alamar Blue assay. The total cell seeding population was kept constant for all the conditions (2×10^6 cells/scaffold). The assays were performed after 1, 3, 5, 7, 9, 11, 13 and 15 days of growth for HBCC and HOLC cultures and 1, 7, 14, 21 days of growth for HBCC and HMSC cultures. For viability studies of the drug treated and non-treated cultures, 3D HBCC, and co-cultures of HBCC and HOLC (1:1), were cultured for 15 days, serum starved for 24 h, treated with 25 μM of Paclitaxel and MTT assay was performed.

Confocal Laser Microscopy, Morphology and Live Image Analysis of Cells: Attachment and spreading of HBCCs, HOLCs and HMSCs (mono-cultures and co-culture) on *A. mylitta* silk fibroin 3D scaffolds was assessed using confocal microscopy. The constructs were imaged by using a confocal laser scanning microscope (CLSM, Olympus FV 1000 attached with inverted microscope IX 81, Japan) equipped with Argon (488 nm) and He–Ne (534 nm) lasers. Two-dimensional multichannel image processing was carried out by FV 1000 Advance software version 4.1 (Olympus, Japan). Cell length was measured with the help of this software. In case of phase contrast microscopy, cell length was measured after calibrating the images with the help of haemocytometer and stage micrometer using Image J software.

For cell morphology, samples were fixed in paraformaldehyde (4%) for 15 min, followed by membrane permeabilisation in Triton X-100 (0.2%) in PBS for 15 min. Samples were then incubated with phalloidin-rhodamine 415 (0.8 U/mL) and the cell nuclei were stained using Hoechst 33342 (5 μg/mL).

For live cell imaging for studying cancer cell migration into osteoblast-like constructs, HOLCs and HBCCs were pre-labeled with CellTracker Green CMFDA (5-chloromethylfluorescein diacetate; Invitrogen, 50 μg) and CellTracker Red CMTPX (Invitrogen, 50 μg), respectively, per manufacturer's instructions prior to seeding. Pre-labeled MG-63 cells (2×10^6 cells) were seeded on *A. mylitta* scaffolds and cultured for 7 days. Pre-labeled MDA-MB-231 (10^6 cells) were seeded on a 6-well plate and cultured for 1 day. These pre-labeled HBCC and HOLC were co-cultured indirectly (**Scheme 4**) for 1, 3, 5 and 7 days. The basal portion of the HOLC seeded scaffolds was analyzed for presence of HBCCs after 1, 3, 5 and 7 days of culture. Confocal images were obtained, stacked and analyzed.

ELISA Studies of 3D Mono and Co-Cultures: The amount of VEGF, IL-8, TGF-β2 and bFGF present in the media samples was determined using the Assay Kit from R&D systems. This assay employs the quantitative sandwich enzyme immunoassay technique. The microplate was pre-coated with monoclonal antibody specific for TGF-β2 and bFGF.

RNA Extraction and RT-PCR for Gene Expression Analysis: Total RNA from co-culture and control constructs was extracted using TRI Reagent (Sigma), precipitated in isopropanol and solubilized in PCR water. RNA was quantified using a Nanodrop ND-1000 (Nanodrop products, Wilminton DE, USA) spectrophotometer and cDNA was reverse transcribed from 1 μg of RNA using random hexanucleotide primers and superscript III reverse transcriptase from RevertAid First Strand cDNA synthesis kit (Fermentas LifeSciences, Germany). Gene expression of MMP-9, RANKL, CASR and GAPDH were studied by semi-quantitative methods using Taq DNA polymerase and real-time quantitative methods by SYBR-green PCR mastermix by following the manufacturer's protocol (Applied Biosystems, USA). Real-time PCR reactions of cDNA samples (50 μL) were run on an ABI Prism 7000 Sequence Detection System (Applied Biosystems, USA) in triplicate and quantitative analysis performed and normalized to GAPDH, FW;

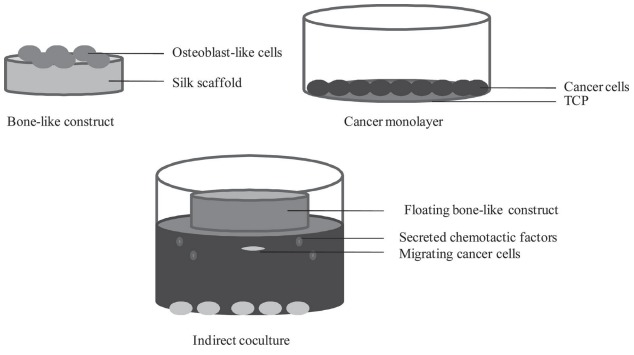

Scheme 4. Schematic representation of indirect co-culture. Bone constructs and cancer monolayers were cultured separately for 15 days. Then the bone-like construct was placed floating over the monolayer.

ATGGGGAAGGTGAAGGTCG, RV; GGGGTCATTGATGGCAACAATA. Target gene expressions were calculated as $2^{-\Delta\Delta Ct}$. The following primer sequences were obtained using the PrimerBank website (http://pga.mgh.harvard.edu/primerbank/):

MMP-9
FW: GGGACGCAGACATCGTCATC
RV: TCGTCATCGTCGAAATGGGC
RANKL
FW: ATCGTTGGATCACAGCACATC
RV: AGACTCACTTTATGGGAACCAGA
CASR
FW: ACCAGCGAGCCCAAAAGAAG
RV: GCGAAACCCACGGAAATTATAC

All primers were obtained from Sigma. The samples were incubated at 25 °C for 10 min, and then RT-PCR was performed at 95 °C for 10 min followed by 40 cycles of 1 min denaturation at 95 °C, 30 s annealing at the primer specific temperature, and elongation at 54 °C for 1 min and 72 °C for 30 s.

Alkaline Phosphatase Activity: The constructs were grown for 21 days and then incubated with incomplete media for 24 h. Culture medium was removed from the co-cultures and controls. The obtained medium was used for the measurement of alkaline phosphatase (AP) activity by Kind and King's method (Cogent alkaline phosphatase diagnostic reagent kit, India) and total protein concentration according to manufacturer's protocol. Alkaline phosphatase from sample converts phenyl phosphate in the reagent to inorganic phosphate and phenol at pH 10.0. Phenol so formed reacts in alkaline medium with 4-aminoantipyrine in presence of the oxidizing agent potassium ferricyanide and forms an orange-red coloured complex, which can be measured colorimetrically. The colour intensity is proportional to the enzyme activity. The AP activity was determined by measuring the absorbance of the orange-red complex at 510 nm and total protein content was determined by Bradford Assay at 540 nm, using a microplate reader (Bio-Rad).

Alizarin Red Assay: 3D silk constructs cultured for 21 days were assessed for extracellular matrix mineralization. Calcium deposition was visualized using Alizarin Red S stain (Sigma–Aldrich, USA). Stain solution was prepared by dissolving Alizarin powder (2 g in 100 mL distilled water). The pH was maintained between 4.1 and 4.3 using ammonium hydroxide solution. Scaffolds fixed in paraformaldehyde (4%) for 15 min, cut into sections, rinsed in PBS and stained in Alizarin Red S solution for 2 min. Excess stain was removed and the stained sections were mounted on slides and analyzed.

Chemotherapeutic Studies: HBCC and HOLC were directly co-cultured at cell ratio of 1:1 in a culture media constituted of DMEM/F-12 and MEM (1:1) and mono-cultures of HBCCs (1:0) or HOLCs (0:1) served as controls. Cell suspensions were prepared at appropriate ratio and cells were seeded in 24-well plates containing *A.mylitta* fibroin scaffolds at 2×10^6 cells/scaffold. Cells were kept at 37 °C in CO_2 incubator for attachment for 24 h prior to drug treatment; the cells were cultured in incomplete media for 24 h. The IC_{50} of paclitaxel was calculated separately.[47] The cultures were treated with 50 μM of Paclitaxel for 48 h. MTT assay was conducted to the cell viability under different culture conditions.

Statistical Analysis: Statistical analysis of the data was performed by one-way analysis of variance (ANOVA) and Students t-test. By conventional criteria, the difference is considered to be statistically significant when $P \leq 0.05$ and highly significant when $P \leq 0.01$. All quantitative experiments were run in triplicate and the results are expressed as means ± standard deviation for $n = 3$, unless indicated otherwise.

Supporting Information

Supporting Information is available from the Wiley Online Library or from the author.

Acknowledgements

This work is supported by Department of Biotechnology and its Bioinformatics facilities, Department of Science and Technology, Government of India. We are also thankful to the subject experts of Indian Council of Medical Research, New Delhi for helpful discussions and suggestions during the initiation of the work.

Received: January 25, 2013
Revised: March 19, 2013
Published online: May 2, 2013

[1] S. S. Verbridge, E. M. Chandler, C. Fischbach, *Tissue Eng. Part A* **2010**, *16*, 2147.
[2] J. A. Joyce. *Cancer Cells* **2005**, *7*, 513.
[3] J. Rice, *Nature* **2012**, *485L*, S55.
[4] Z. I. Khamis, Z. J. Sahab, Q. X. A. Sang, *Int. J. Breast Cancer* **2012**, *2012*, 574025.
[5] Z. W. Li, W. S. Dalton, *Blood Rev.* **2006**, *20*, 333.
[6] T. A. Guise, *Cancer Treat. Rev.* **2008**, *34*, S19.
[7] S. P. Pathi, C. Kowalczewski, R. Tadipatri, C. Fischbach, *PLoS One* **2010**, *5*, e8849.
[8] I. J. Fidler, *Nat. Rev. Cancer* **2003**, *3*, 453.
[9] A. F. Chambers, A. C. Groom, I. C. MacDonald, *Nat. Rev. Cancer* **2002**, *2*, 563.
[10] J. A. Joyce, J. W. Pollard, *Nat. Rev. Cancer* **2009**, *9*, 239.
[11] P. Gassmann, J. Haier, G. L. Nicolson, *Cancer Growth Progr.* **2008**, *11*, 21.
[12] A. Müller, B. Homey, H. Soto, N. Ge, D. Catron, M. E. Buchanan, T. McClanahan, E. Murphy, W. Yuan, S. N. Wagner, J. L. Barrera, A. Mohar, E. Verástegui, A. Zlotnik, *Nature* **2001**, *410*, 50.
[13] A. Zlotnik, *Semin. Cancer Biol.* **2004**, *14*, 181.
[14] J. G. Jackson, X. Zhang, T. Yoneda, D. Yee, *Oncogene* **2001**, *20*, 7318.
[15] R. Nicholson, G. Murphy, R. Breathnach, *Biochemistry* **1989**, *28*, 5195.
[16] G. Giannelli, C. Bergamini, E. Fransvea, F. Marinosci, V. Quaranta, S. Antonaci, *Lab. Invest.* **2001**, *81*, 613.
[17] M. Morini, M. Mottolese, N. Ferrari, F. Ghiorzo, S. Buglioni, R. Mortarini, D. M. Noonan, P. G. Natali, A. Albini, *Int. J. Cancer* **2000**, *87*, 336.
[18] G. R. Mundy, *Nat. Rev. Cancer* **2002**, *2*, 584.
[19] S. P. Pathi, D. D. W. Lin, J. R. Dorvee, L. A. Estroff, C. Fischbach, *Biomaterials* **2011**, *32*, 5112.
[20] K. M. Bussard, C. V. Gay, A. M. Mastro, *Cancer Metastasis Rev.* **2008**, *27*, 41.
[21] G. R. Mundy, *Nutr. Rev.* **2007**, *65*, S147.
[22] A. Leibbrandt, J. M. Penninger, *Ann. NY Acad. Sci.* **2008**, *1143*, 123.
[23] E. Y. Lin, V. Gouon-Evans, A. V. Nguyen, J. W. Pollard, *J. Mammary Gland Biol. Neoplasia* **2002**, *7*, 147.
[24] D. H. Jones, T. Nakashima, O. H. Sanchez, I. Kozieradzki, S. V. Komarova, I. Sarosi, S. Morony, E. Rubin, R. Sarao, C. V. Hojilla, V. Komnenovic, Y. Y. Kong, M. Schreiber, S. J. Dixon, S. M. Sims, R. Khokha, T. Wada, J. M. Penninger, *Nature* **2006**, *440*, 692.
[25] R. Mihai, *Ann. R. Coll. Surg. Engl.* **2008**, *90*, 271.
[26] J. L. Sanders, N. Chattopadhyay, O. Kifor, T. Yamaguchi, R. R. Butters, E. M. Brown, *Endocrinology* **2000**, *141*, 4357.
[27] L. Qiao, Z. Xu, T. Zhao, Z. Zhao, M. Shi, R. C. Zhao, L. Ye, X. Zhang, *Cell Res.* **2008**, *18*, 500.
[28] K. E. Corcoran, K. A. Trzaska, H. Fernandes, M. Bryan, M. Taborga, V. Srinivas, K. Packman, P. S. Patel, P. Rameshwar, *PLoS One* **2008**, *3*, e2563.
[29] F. Dazzi, R. Ramasamy, S. Glennie, S. P. Jones, I. Roberts, *Blood Rev.* **2006**, *20*, 161.

[30] J. E. Moreau, K. Anderson, J. R. Mauney, T. Nguyen, D. L. Kaplan, M. Rosenblatt, *Cancer Res.* **2007**, *67*, 10304.
[31] D. W. Hutmacher, *Nat. Mater.* **2010**, *9*, 90.
[32] D. W. Hutmacher, D. Loessner, S. Rizzi, D. L. Kaplan, D. J. Mooney, J. A. Clements, *Trends Biotechnol.* **2010**, *28*, 125.
[33] E. Burdett, F. K. Kasper, A. G. Mikos, J. A. Ludwig, *Tissue Eng. Part. B Rev.* **2010**,*16*, 351.
[34] B. B. Mandal, S. C. Kundu, *Macromol. Biosci.* **2008**, *8*, 807.
[35] B. B. Mandal, S. C. Kundu, *Biomaterials* **2009**, *30*, 2956.
[36] S. Talukdar, Q. T. Nguyen, A. C. Chen, R. L. Sah, S. C. Kundu, *Biomaterials* **2011**, *32*, 8927.
[37] S. Talukdar, M. Mandal, D. W. Hutmacher, P. J. Russell, C. Soekmadji, S. C. Kundu, *Biomaterials* **2011**, *32*, 2149.
[38] B. B. Mandal, S. C. Kundu, *Biotechnol. Bioeng.* **2008**, *100*, 1250.
[39] R. Nazarov, H. J. Jin, D. L. Kaplan. *Biomacromolecules* **2004**, *5*, 726.
[40] A. Datta, A. K. Ghosh, S. C. Kundu, *Comp. Biochem. Physiol. B – Biochem. Mol. Biol.* **2001**, *129*, 204.
[41] Y. Q. Zhang, W. L. Zhou, W. D. Shen, Y. H. Chen, X. M. Zha, K. Shirai, K. Kiguchi, *J. Biotechnol.* **2005**, *120*, 326.
[42] L. Meinel, S. Hofmann, V. Karageorgiou, C. Kirker-Head, J. McCool, G. Gronowicz, L. Zichner, R. Langer, G. Vunjak-Novakovic, D. L. Kaplan, *Biomaterials* **2005**, *26*, 155.
[43] E. L. Baker, J. Lu, D. Yu, R. T. Bonnecaze, M. H. Zaman, *Biophys. J.* **2010**, *99*, 2057.
[44] J. T. Erler, V. M. Weaver, *Clin. Exp. Metastasis* **2009**, *26*, 49.
[45] K. R. Levental, H. Yu, L. Kass, J. N. Lakins, M. Egeblad, J. T. Erler, S. F. Fong, K. Csiszar, A. Giaccia, W. Weninger, M. Yamauchi, D. L. Gasser, V. M. Weaver, *Cell* **2009**, *139*, 906.
[46] A. L. McKnight, J. L. Kugel, P. J. Rossman, A. Manduca, L. C. Hartmann, R. L. Ehman, *AJR* **2002**, *178*, 1417.
[47] S. Talukdar, S. C. Kundu, *Adv. Funct. Mater.* **2012**, *22*, 4778.
[48] B. B. Mandal, S. C. Kundu, *Acta Biomater.* **2009**, *5*, 2579.
[49] W. Pradel, R. Mai, T. Gedrange, G. Lauer, *J. Physiol. Pharmacol.* **2008**, *59*, 58.
[50] J. Ma, J. J. van den Beucken, F. Yang, S. K. Both, F. Z. Cui, J. Pan, J. A. Jansen, *Tissue Eng. Part C Methods* **2011**, *17*, 57.
[51] M. Lacroix, B. Siwek, J. J. Body, *Breast Cancer Res. Treat.* **1996**, *38*, 209.
[52] R. J. Thomas, T. A. Guise, J. J. Yin, J. Elliott, N. J. Horwood, T. J. Martin, M. T. Gillespie, *Endocrinology* **1999**, *140*, 4451.
[53] A. M. Mastro, C. V. Gay, D. R. Welch, H. J. Donahue, J. Jewell, R. Mercer, D. DiGirolamo, E. M. Chislock, K. Guttridge, *J. Cell Biochem.* **2004**, *91*, 265.
[54] C. Secondini, A. Wetterwald, R. Schwaninger, G. N. Thalmann, M. G. Cecchini, *PLoS One* **2011**, *6*, e16078.
[55] M. A. Karsdal, M. S. Fjording, N. T. Foged, J. M. Delaissé, A. Lochter, *J. Biol. Chem.* **2001**, *276*, 39350.
[56] D. M. Sosnoski, V. Krishnan, W. J. Kraemer, C. Dunn-Lewis, A. M. Mastro, *Int. J. Breast Cancer* **2012**, *2012*, 160265.
[57] P. Clézardin, *Breast Cancer Res.* **2011**, *13*, 207.
[58] M. B. Meads, R. A. Gatenby, W. S. Dalton, *Nat. Rev. Cancer* **2009**, *9*, 665.
[59] R. Sapir-Koren, G. Livshits, *IBMS BoneKEy* **2011**, *8*, 86.
[60] M. A. S. Moore, *Bioessays* **2001**, *23*, 674.
[61] Z. Saidak, C. Boudot, R. Abdoune, L. Petit, M. Brazier, R. Mentaverri, S. Kamel, *Exp. Cell Res.* **2009**, *315*, 2072.
[62] T. A. Guise, BoneKEy-Osteovision, **2002**, DOI:10.1138/2002052.
[63] K. Jacob, M. Webber, D. Benayahu, H. K. Kleinman, *Cancer Res.* **1999**, *59*, 4453.
[64] S. A. Patel, A. C. Heinrich, B. Y. Reddy, B. Srinivas, N. Heidaran, P. Rameshwar, *J. Oncol.* **2008**, *425895*, 7.
[65] H. M. Berghuis, S. C. Dieudonné, W. Goei, J. P. Veldhuijzen, *Eur. J. Orthod.* **1994**, *16*, 130.
[66] L. Marinucci, S. Balloni, E. Becchetti, G. Bistoni, E. M. Calvi, E. Lumare, F. Ederli, P. Locci, *Ann. Biomed. Eng.* **2010**, *38*, 640.
[67] V. Levina, A. M. Marrangoni, R. DeMarco, E. Gorelik, A. E. Lokshin, *PLoS ONE* **2008**, *3*, e3077.
[68] D. Marzioni, T. Lorenzi, R. Mazzucchelli, L. Capparuccia, M. Morroni, R. Fiorini, C. Bracalenti, A. Catalano, G. David, M. Castellucci, G. Muzzonigro, R Montironi, *Int. J. Immunopathol. Pharmacol.* **2009**, *22*, 627.
[69] D. Fang, T. K. Nguyen, K. Leishear, R. Finko, A. N. Kulp, S. Hotz, P. A. Van Belle, X. Xu, D. E. Elder, M. Herlyn, *Cancer Res.* **2005**, *65*, 9328.
[70] T. Ohshiba, C. Miyaura, M. Inada, A. Ito, *Br. J. Cancer* **2003**, *88*, 1318.